Kishal Bipin Tandel
23MS115
September 25, 2025

Report 2

Instructors:
Prof. Satyabrata Raj
Prof. Goutam D. Mukherjee

PH3105: Nuclear Physics Laboratory

Abstract

In this experiment, the γ ray energy spectrum of a ^{137}Cs source was studied using a NaI(Tl) scintillation detector coupled to a photomultiplier tube (PMT) and a Single Channel Analyzer (SCA). The resulting spectrum shows the photopeak, Compton continuum, Compton edge, backscatter features, backscatter peak and Ba K-X ray peak. The energy resolution of the detector was determined from the full width at half maximum (FWHM) of the photopeak.

Contents

1 Introduction

This report documents a laboratory experiment designed to measure and analyse the energy spectrum of gamma radiation using a NaI(Tl) scintillation detector coupled to a photomultiplier tube (PMT) and a Single Channel Analyzer (SCA). The measurements performed in this experiment are fundamental to nuclear spectroscopy: they allow identification of radionuclides by their characteristic gamma lines, assessment of detector performance (energy resolution and efficiency), and demonstration of the physical processes that shape the observed spectrum.

1.1 Aim

The aims of the experiment are as follows:

1. To record the pulse-height (energy) spectrum of ^{137}Cs using a NaI(Tl) scintillation detector and an SCA-based scanning technique.
2. To determine the full-energy peak energy resolution at observed photopeak.

1.2 Apparatus and Materials

The source of γ ray photons in this experiment was radioactive ^{137}Cs. The detector was NaI(Tl) scintillation crystal which was optically coupled to a PMT and SCA. We also used an oscilloscope for monitoring pulse shapes .

1.3 Experimental Setup and ^{137}Cs Source

The experimental set up and ^{137}Cs source are shown in Figure 1.

Figure 1: Experimental setup (left) and ^{137}Cs source (right)

2 Theory

2.1 Photon interactions with matter

Photons are quanta of electromagnetic radiation characterized by zero rest mass, no electric charge, and constant velocity c, the speed of light. Unlike charged particles, which continuously lose energy through Coulombic interactions with matter, photons travel considerable distances without significant energy loss. Instead, they interact with matter through distinct mechanisms that result in partial or complete energy transfer to electrons. These secondary electrons subsequently deposit energy locally within the medium. Owing to this nature, photons are significantly more penetrating than charged particles of comparable energy.

The primary mechanisms by which photons interact with matter are the **photoelectric effect**, **Compton scattering**, and **pair production**. The probability of these interactions is quantified by the *linear attenuation coefficient* μ, which gives the probability of interaction per unit path length. It is material- and energy-dependent and is commonly expressed in units of cm^{-1}. By normalizing with respect to density ρ, one obtains the *mass attenuation coefficient* μ/ρ, expressed in cm^2/g.

2.1.1 Photoelectric effect

The photoelectric interaction results in the complete absorption of the incident photon and the ejection of a bound atomic electron. In the photoelectric process, a photon is completely absorbed by an atom, resulting in the ejection of an electron from an inner shell, typically the K-shell if the incident photon energy is sufficiently high. The kinetic energy of the emitted photoelectron is given by

$$E_{e^-} = h\nu - E_b$$

where $h\nu$ is the photon energy and E_b is the binding energy of the electron. The resulting vacancy in the atomic shell may lead to the emission of characteristic fluorescence X-rays. The photoelectric effect dominates at relatively low photon energies and for materials with high atomic number Z. Its probability τ is approximately proportional to

$$\tau \propto \frac{Z^n}{(h\nu)^3}, \quad \text{with } n \in [3, 4]$$

This strong Z-dependence explains why high-Z materials, such as lead, are effective shielding agents for low-energy photons. Photoelectric absorption is responsible for the full-energy (photo)peak in a detector when the entire photon energy is deposited. A schematic of Photoelectric Effect is shown in Figure 2.

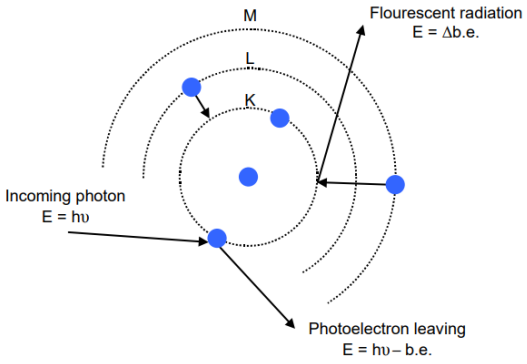

Figure 2: Schematic of Photoelectric Effect

2.1.2 Compton scattering

Compton scattering involves an inelastic collision between a photon and an essentially free or loosely bound electron. The photon is scattered at an angle θ relative to its incident direction, and a recoil electron (Compton electron) is ejected. The scattered photon has reduced energy,

$$h\nu' = \frac{h\nu}{1 + \frac{h\nu}{m_e c^2}(1 - \cos\theta)}$$

The corresponding energy imparted to the recoil electron is

$$E_{e^-} = h\nu - h\nu' = h\nu \left[1 - \frac{1}{1 + \frac{h\nu}{m_e c^2}(1 - \cos\theta)}\right]$$

The maximum kinetic energy transferred to the electron (Compton edge) occurs for backscatter $\theta = \pi$ and is given by

$$E_{e^-,\max} = h\nu \left(1 - \frac{1}{1 + \frac{2h\nu}{m_e c^2}}\right)$$

Compton scattering produces the continuous distribution below the photopeak with a sharp cutoff at the Compton edge. The Compton process is dominant in the intermediate energy range (100 keV–10 MeV) and is particularly significant for photon interactions in soft tissues. Its probability, denoted by σ, is nearly independent of Z, depending primarily on electron density. A schematic of Compton Scattering is shown in Figure 3.

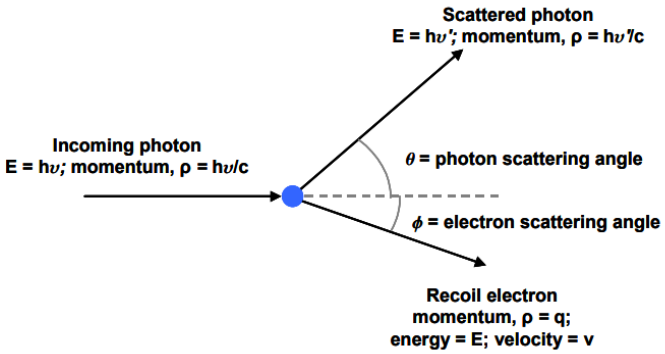

Figure 3: Schematic of Compton Scattering

2.1.3 Pair Production

When photon energy exceeds 1.022 MeV, interaction with the Coulomb field of a nucleus can lead to pair production. In this process, the photon disappears and is converted into an electron–positron pair:

$$h\nu \rightarrow e^- + e^+$$

The threshold energy corresponds to twice the electron rest energy ($2m_e c^2 = 1.022$ MeV). The kinetic energy of the created particles is

$$E_{e^-} + E_{e^+} = h\nu - 1.022\,\text{MeV}$$

The probability of pair production κ increases with photon energy and is approximately proportional to Z^2. The positron will eventually annihilate with an electron, producing two photons of 0.511 MeV each; if one or both of these annihilation photons escape the detector volume, escape peaks at $h\nu - 511$ keV (single-escape) and $h\nu - 1022$ keV (double-escape) appear in the spectrum. A schematic of Pair Production is shown in Figure 4.

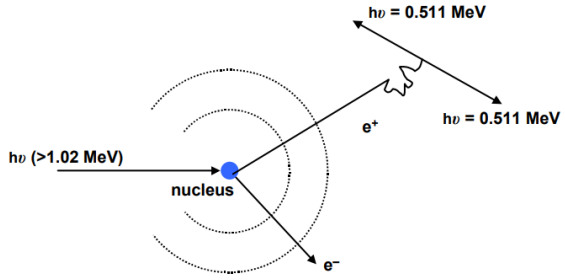

Figure 4: Schematic of Pair Production

2.1.4 Bulk Attenuation and Energy Deposition

The total attenuation coefficient is the sum of the contributions from all three processes:

$$\mu = \tau + \sigma + \kappa$$

Not all photon energy transferred to matter is absorbed locally. Some may escape as fluorescence photons or bremsstrahlung radiation. To describe the effective dose, one defines the energy-transfer coefficient μ_{tr} and the energy-absorption coefficient μ_{en}, where

$$\mu_{en} = \mu_{tr}(1 - g)$$

with g representing the fraction of transferred energy that escapes as radiative losses. The parameter μ_{en}/ρ is especially important in medical physics and radiation protection, as it directly relates to the absorbed dose.

In conclusion, photon interactions in matter are governed by three principal mechanisms, each dominating different energy regimes and showing distinct dependencies on photon energy and atomic number. These processes collectively determine photon penetration, shielding effectiveness, and energy deposition, which are crucial in fields such as diagnostic radiology, nuclear medicine, radiation therapy, and radiation shielding design. The plot showing the dominance of each of these three principal mechanisms in different energy regimes and for different atomic numbers is shown in Figure 5.

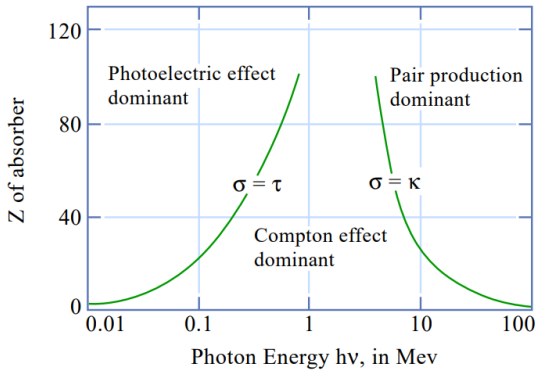

Figure 5: Atomic Number Z vs. Energy $h\nu$ (MeV)

2.2 Decay Scheme of ^{137}Cs

Cesium-137 (^{137}Cs) is a radioactive fission product with a half-life of

$$T_{1/2} = 30.17 \text{ years}$$

It decays predominantly by β^- emission to an excited state of barium-137 ($^{137\text{m}}$Ba), which then de-excites by emitting a characteristic gamma ray. The overall decay scheme is therefore a two-step process: a nuclear β^- decay followed by an electromagnetic de-excitation.

2.2.1 Beta Decay

The primary decay mode of ^{137}Cs is β^- decay, in which a neutron in the nucleus transforms into a proton, accompanied by the emission of an electron (the beta particle) and an antineutrino:

$$n \;\rightarrow\; p + e^- + \bar{\nu}_e$$

At the nuclear level, this transforms ^{137}Cs (Z=55) into an excited state of ^{137}Ba (Z=56). The reaction can be written as

$$^{137}_{55}\text{Cs} \;\rightarrow\; ^{137\text{m}}_{56}\text{Ba}^* + e^- + \bar{\nu}_e$$

About 94.6% of the decays populate the metastable isomeric state $^{137\text{m}}$Ba at 661.7 keV excitation energy. A much smaller fraction ($\sim$ 5.4%) directly populates the ground state of ^{137}Ba. The endpoint energy of the emitted beta spectrum in the main branch is approximately 1.176 MeV, while in the minor branch it is about 514 keV.

2.2.2 Isomeric Transition and Gamma Emission

The metastable $^{137\text{m}}$Ba state has a half-life of

$$T_{1/2} = 2.55 \text{ minutes}$$

It de-excites almost exclusively via electromagnetic processes. The most probable mode is gamma emission, in which a 661.7 keV photon is emitted:

$$^{137\text{m}}_{56}\text{Ba} \;\rightarrow\; ^{137}_{56}\text{Ba}_{(\text{ground})} + \gamma\,(661.7 \text{ keV})$$

This 662 keV gamma ray is the prominent line observed in scintillation spectroscopy of ^{137}Cs and is the basis for its widespread use as a calibration source in gamma-ray detectors.

2.2.3 Internal Conversion

In addition to gamma-ray emission, the excited $^{137\text{m}}$Ba nucleus can also decay via the process of internal conversion. In this process, instead of emitting a gamma ray, the nucleus transfers its excitation energy directly to one of its own orbital electrons, which is then ejected from the atom:

$$^{137\text{m}}_{56}\text{Ba} \;\rightarrow\; ^{137}_{56}\text{Ba}_{(\text{ground})} + e^-_{\text{IC}}$$

The probability of internal conversion relative to gamma emission is described by the *internal conversion coefficient* (ICC), defined as

$$\alpha = \frac{N_{\text{IC}}}{N_\gamma}$$

where N_{IC} is the number of internal conversion electrons and N_γ is the number of gamma photons emitted. For $^{137\text{m}}$Ba, the ICC for the 661.7 keV transition is approximately $\alpha \approx 0.12$. Thus, about 12% as many conversion electrons are emitted as gamma rays. The ejection of inner-shell electrons also leads to the emission of characteristic X-rays from barium as the atomic vacancies are filled.

2.2.4 Summary of Decay Scheme

The complete decay scheme of ^{137}Cs can be summarized as follows:

$$
\begin{aligned}
{}^{137}_{55}\mathrm{Cs} &\xrightarrow[\beta^-,\,94.6\%]{T_{1/2}=30.17\,\mathrm{y}} {}^{137\mathrm{m}}_{56}\mathrm{Ba}\,(661.7\ \mathrm{keV}) + e^- + \bar{\nu}_e \\
{}^{137\mathrm{m}}_{56}\mathrm{Ba} &\xrightarrow[\gamma,\,85.1\%]{T_{1/2}=2.55\,\mathrm{min}} {}^{137}_{56}\mathrm{Ba}_{(\mathrm{g.s.})} + \gamma\,(661.7\ \mathrm{keV}) \\
{}^{137\mathrm{m}}_{56}\mathrm{Ba} &\xrightarrow[\mathrm{IC},\,11\%]{} {}^{137}_{56}\mathrm{Ba}_{(\mathrm{g.s.})} + e^-_{\mathrm{IC}} \\
{}^{137}_{55}\mathrm{Cs} &\xrightarrow[\beta^-,\,5.4\%]{} {}^{137}_{56}\mathrm{Ba}_{(\mathrm{g.s.})} + e^- + \bar{\nu}_e
\end{aligned}
$$

Thus, the ^{137}Cs decay chain provides a nearly monoenergetic 662 keV gamma ray with high intensity, making it an ideal source for energy calibration in gamma spectroscopy.

2.3 NaI(Tl) Scintillation Detector

The fundamental principle of a scintillation detector is the conversion of ionizing radiation into visible light photons, which can then be detected by a photosensitive device. In this experiment, a thallium-doped sodium iodide [NaI(Tl)] scintillation crystal is used. Sodium iodide is an inorganic scintillator with a high atomic number ($Z = 53$ for iodine), giving it a large photoelectric cross-section and therefore high detection efficiency for medium-energy gamma rays such as the 662 keV photon from ^{137}Cs. The addition of thallium, in concentrations of approximately 0.1% by weight, introduces activator sites in the crystal lattice that are essential for efficient scintillation.

When a gamma ray enters the NaI(Tl) crystal, it interacts with the material via one of the standard gamma-ray interaction mechanisms: the photoelectric effect, Compton scattering, or pair production (though the latter is absent at 662 keV). In each case, energetic secondary electrons are produced. These electrons lose their energy primarily through ionization and excitation of the crystal lattice. The excitation energy is then transferred to the thallium activator sites. The excited thallium ions subsequently return to their ground state by emitting photons in the visible region, typically centered around 410 nm. This emission is well matched to the spectral sensitivity of photomultiplier tubes.

The NaI(Tl) scintillator has several important characteristics that make it suitable for gamma spectroscopy. Firstly, it exhibits a high light yield, approximately 38,000 photons per MeV of absorbed gamma-ray energy, which translates to good energy resolution. Secondly, its scintillation decay time is relatively short (around 230 ns), allowing for the detection of events at high counting rates. Thirdly, NaI(Tl) crystals can be manufactured in large sizes, increasing detection efficiency for weak or extended sources. However, the material is hygroscopic and readily absorbs moisture from the atmosphere, so the crystal must be hermetically sealed in an aluminum housing with a transparent optical window for coupling to the photomultiplier tube. In the present experiment, the NaI(Tl) scintillator is responsible for converting the discrete gamma-ray energies of ^{137}Cs into flashes of light proportional to the deposited energy.

2.4 Photomultiplier Tube (PMT)

The scintillation light emitted by the NaI(Tl) crystal is too faint to be measured directly using ordinary electronics. Therefore, it is coupled optically to a photomultiplier tube (PMT), which acts

as an extremely sensitive light detector with high gain. A PMT consists of three main functional components: a photocathode, a series of dynodes, and an anode.

The photocathode is a thin photosensitive layer deposited on the inner surface of the PMT window. When photons from the scintillator strike the photocathode, they liberate electrons via the photoelectric effect. The probability of photon-to-electron conversion is described by the quantum efficiency of the photocathode, which is typically in the range of 20–30% at 410 nm for commonly used bialkali photocathodes. The emitted electrons are referred to as photoelectrons, and the number of photoelectrons generated is directly proportional to the intensity of the scintillation light, and hence to the energy deposited in the scintillator by the gamma ray.

The photoelectrons are then accelerated and focused onto the first dynode by an applied high voltage (usually several hundred to over one thousand volts across the tube). When a photoelectron strikes the dynode, secondary emission occurs: several electrons are ejected for each incident electron. This multiplication process is repeated at each successive dynode stage, with typical PMTs containing 8 to 14 dynodes. The overall electron multiplication, or gain, can be as high as 10^6 to 10^7, amplifying the signal from just a handful of photoelectrons to a measurable current pulse. The final electron cloud is collected at the anode, resulting in a sharp voltage pulse at the PMT output. The amplitude of this pulse is proportional to the original energy deposition in the scintillator, allowing pulse-height spectroscopy to be performed.

The PMT is therefore an indispensable part of the scintillation detection system. It combines high sensitivity to single photons, large internal gain, and nanosecond time resolution. However, it is also sensitive to noise such as thermionic emission from the photocathode (dark current) and afterpulsing. Proper biasing of the PMT and shielding from ambient light are essential for stable operation. In this experiment, the PMT provides the electrical pulses that carry the gamma-ray energy information after detection in the scintillator.

2.5 Single Channel Analyzer (SCA)

The electrical output of the photomultiplier tube consists of pulses of varying amplitudes. Each pulse amplitude is proportional to the energy deposited in the scintillator by an incident gamma ray. However, to extract useful spectral information from these pulses, further electronic processing is required. For this purpose, a Single Channel Analyzer (SCA) is employed in the experiment.

An SCA functions as an amplitude discriminator that allows only those pulses whose heights fall within a specific window to pass. By incrementally shifting this discriminator window across the pulse amplitude distribution, the gamma-ray spectrum can be reconstructed point by point. This method is particularly suitable for educational laboratory experiments, where a full multichannel analyzer (MCA) may not be available.

In the case of the ^{137}Cs spectrum, the use of the SCA enables one to observe the Compton continuum, which arises from incomplete energy deposition by Compton scattering, and the distinct photopeak at 662 keV, which results from full absorption of the incident gamma ray via the photoelectric effect following multiple Compton scatterings. The Compton edge, corresponding to the maximum energy transferable to an electron in a single Compton interaction, is also visible. By measuring the width of the photopeak, the energy resolution of the NaI(Tl)-PMT system can be determined. The SCA thus plays a crucial role in gamma-ray spectroscopy, serving as the energy-selective filter that transforms the raw PMT output into meaningful spectral data.

2.6 Energy Resolution of the Scintillation Detector

One of the key performance characteristics of a scintillation spectrometer is its **energy resolution**, which quantifies the detector's ability to distinguish between two gamma rays of closely spaced energies. In practice, when a monoenergetic gamma ray such as the 661.7 keV photon from ^{137}Cs interacts with the NaI(Tl) detector, the resulting photopeak in the pulse height spectrum is not a sharp line but rather has a finite width. This broadening arises primarily from statistical fluctuations in the number of scintillation photons produced, the number of photoelectrons emitted at the PMT photocathode, and subsequent variations in the electron multiplication process. Additional contributions come from non-uniform light collection within the crystal, electronic noise in the signal chain, and intrinsic properties of the scintillator such as non-proportionality of light yield.

The photopeak in the measured spectrum is generally well described by a Gaussian distribution, with its width characterized by the full width at half maximum (FWHM). The **energy resolution** R of the detector at a gamma-ray energy E is therefore defined as

$$R(E) \;=\; \frac{\Delta E}{E} \times 100\%$$

where ΔE is the FWHM of the photopeak (expressed in the same energy units as E). This definition provides a dimensionless measure of the sharpness of the peak.

From a theoretical standpoint, the energy resolution is ultimately limited by the statistics of photon generation and detection. If N represents the average number of photoelectrons produced per absorbed gamma ray, then the statistical fluctuation in this number follows Poisson statistics, with standard deviation $\sqrt{N}$. The corresponding relative uncertainty scales as $1/\sqrt{N}$. Since N is proportional to the deposited energy E, the statistical contribution to the resolution is expected to scale as

$$R(E) \;\propto\; \frac{1}{\sqrt{E}}$$

This dependence explains why scintillation detectors have better (i.e., smaller) resolution at higher gamma-ray energies.

In practice, the measured energy resolution of NaI(Tl) detectors at 662 keV is typically in the range of 6–10%, depending on the crystal quality, size, optical coupling to the PMT, and electronic processing. While this resolution is inferior to that of semiconductor detectors such as high-purity germanium (HPGe), it is adequate for many applications, particularly when high efficiency and robustness are required.

4 Observation Table

The raw measurements obtained from SCA scan and oscilloscope inspections are listed in the following table:

Sr. No.	Baseline Voltage (in mV)	Count 1 (per 30 s)	Count 2 (per 30 s)	Mean Count (per 30 s)
1	20	1	2	1.5
2	60	10	2	6.0
3	100	11	13	12.0
4	140	11	1	6.0
5	180	0	0	0.0
6	220	125	115	120.0
7	260	1517	1544	1530.5
8	300	5163	4981	5072.0
9	340	7252	7100	7176.0
10	380	3897	4021	3959.0
11	420	2725	2758	2741.5
12	460	2895	2829	2862.0
13	500	4069	4164	4116.5
14	540	8004	8088	8046.0
15	580	16384	16426	16405.0
16	620	18503	18238	18370.5
17	660	20788	21153	20970.5
18	700	21719	21676	21697.5
19	740	22205	22310	22257.5
20	780	21491	21514	21502.5
21	820	18408	18800	18604.0
22	860	15789	16745	16267.0
23	900	18882	25329	22105.5
24	940	6569	6561	6565.0
25	980	5390	5519	5454.5
26	1020	4893	4936	4914.5
27	1060	3766	3815	3790.5
28	1100	3438	3324	3381.0
29	1140	2891	3025	2958.0

Sr. No.	Baseline Voltage (in mV)	Count 1 (per 30 s)	Count 2 (per 30 s)	Mean Count (per 30 s)
30	1180	2681	2721	2701.0
31	1220	2419	2451	2435.0
32	1260	2405	2394	2399.5
33	1300	2202	2197	2199.5
34	1340	2145	2081	2113.0
35	1380	1982	2006	1994.0
36	1420	1971	1998	1984.5
37	1460	1885	1954	1919.5
38	1500	2049	1749	1899.0
39	1540	1844	1795	1819.5
40	1580	1875	1891	1883.5
41	1620	1852	1801	1826.5
42	1660	1972	1768	1870.0
43	1700	1884	1930	1907.0
44	1740	1799	1913	1856.0
45	1780	1931	1870	1900.5
46	1820	1944	1908	1926.0
47	1860	1832	1796	1814.0
48	1900	1705	1701	1703.0
49	1940	1350	1363	1356.5
50	1980	874	875	874.5
51	2020	687	677	682.0
52	2060	551	551	551.0
53	2100	538	540	539.0
54	2140	499	484	491.5
55	2180	466	502	484.0
56	2220	492	564	528.0
57	2260	507	526	516.5
58	2300	507	521	514.0
59	2340	559	517	538.0
60	2380	647	649	648.0
61	2420	805	764	784.5
62	2460	1345	1268	1306.5

Sr. No.	Baseline Voltage (in mV)	Count 1 (per 30 s)	Count 2 (per 30 s)	Mean Count (per 30 s)
63	2500	2357	2448	2402.5
64	2540	4577	4630	4603.5
65	2580	6905	6983	6944.0
66	2620	9626	9834	9730.0
67	2660	9482	9558	9520.0
68	2700	6874	6833	6853.5
69	2740	4787	4629	4708.0
70	2780	1773	1741	1757.0
71	2820	692	648	670.0
72	2860	196	183	189.5
73	2900	139	138	138.5
74	2940	121	108	114.5
75	2980	112	99	105.5
76	3020	77	105	91.0
77	3060	86	93	89.5
78	3100	82	87	84.5
79	3140	77	86	81.5
80	3180	73	80	76.5
81	3220	82	75	78.5
82	3260	80	73	76.5
83	3300	67	83	75.0
84	3340	64	68	66.0
85	3380	57	66	61.5
86	3420	75	59	67.0
87	3460	67	52	59.5
88	3500	51	56	53.5
89	3540	57	50	53.5
90	3580	56	41	48.5

Table 1: Baseline Voltage (mV) vs. Count (per 30 s)

5 Plotting and Data Analysis

5.1 Graph

On plotting Baseline Voltage (mV) vs. Mean Count (per 30 s) from Table 1, identifying and labelling the various peaks and features, we get the following graph:

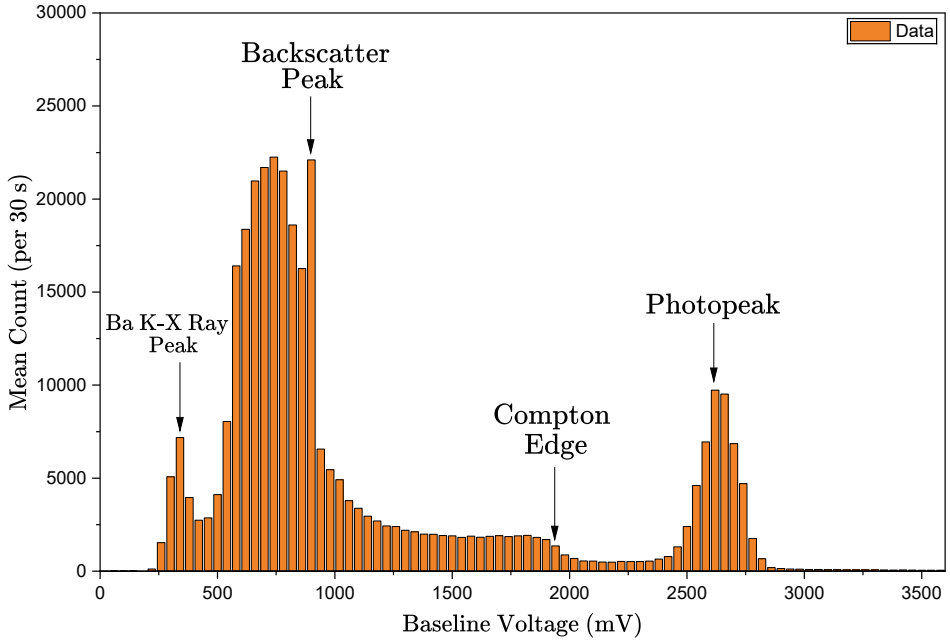

Figure 6: γ ray energy spectrum of ^{137}Cs

5.2 Qualitative Analysis of the Graph

The spectrum shown in Figure 6 is the pulse-height (baseline voltage) spectrum of γ-rays from ^{137}Cs measured with a NaI(Tl) scintillator, PMT and SCA. The horizontal axis (baseline voltage, mV) is proportional to the energy deposited in the scintillator and the vertical axis is counts per fixed live time; therefore the large feature centered at the higher-voltage end of the spectrum is the full-energy (photo-) peak corresponding to the ^{137}Cs primary γ-ray of $E_\gamma = 662\,\text{keV}$. This photopeak arises when the entire γ-ray energy is absorbed in the detector (direct photoelectric absorption or multiple interactions that sum to the full energy).

To the left of the photopeak the spectrum exhibits the Compton continuum terminating at the Compton edge, which corresponds to the maximum kinetic energy transferred to an electron in a single Compton scatter. The Compton scattering relation for a photon of initial energy E scattered through an angle θ is

$$E'(\theta) = \frac{E}{1 + \dfrac{E}{m_e c^2}(1 - \cos\theta)}$$

where E' is the scattered photon energy and $m_e c^2 = 511\,\text{keV}$. The maximum energy given to the recoil electron occurs for $\theta = 180°$ (backscatter) so the Compton edge energy deposited in the

detector (maximum electron energy) is

$$E_{e,\max} = E - E'(180^\circ) = E\left(1 - \frac{1}{1 + \dfrac{2E}{m_e c^2}}\right)$$

For $E = 662\,\text{keV}$ this gives $E'(180^\circ) \approx 184.4\,\text{keV}$ and $E_{e,\max} \approx 477.6\,\text{keV}$; these values map to the voltage of the observed Compton edge (marked on the graph near $\sim 2000\,\text{mV}$). The continuous distribution below the edge is the Compton continuum produced by all scattering angles $0 < \theta < 180^\circ$, where varying fractions of the primary γ-energy are deposited in single or multiple scatters.

A smaller low-energy peak visible near $\sim 400\,\text{mV}$ is the characteristic X-ray (K-X ray) peak from barium/iodine fluorescence. When a γ-ray deposits energy via the photoelectric effect in the iodine (or the crystal/bulk), vacancies in inner shells lead to emission of characteristic K X-rays (Ba Kα/Kβ roughly in the $\sim$30–35 keV range) which, if subsequently absorbed in the crystal, give a small peak at the corresponding lower pulse height. This satellite peak confirms the presence of inner-shell fluorescence and is commonly observed with NaI(Tl) detectors coupled to mid-energy sources.

A prominent feature on the lower-voltage side of the Compton continuum is the backscatter peak (marked near $\sim 900\,\text{mV}$). This arises from photons that undergo a large-angle (180°) Compton scatter in surrounding materials (shielding, table, detector housing, etc.) and then enter the detector with reduced energy $E'(180^\circ)$. The backscattered photon may then deposit most or part of its remaining energy in the crystal by photoelectric absorption or further Compton interactions. For ^{137}Cs the backscattered photon energy $E'(180^\circ) \approx 184\,\text{keV}$, so the backscatter peak appears at a lower voltage than the full-energy peak. The existence and amplitude of this peak depend strongly on geometry and surrounding material: a solid, high-Z scatterer near the crystal produces more backscattered photons and hence a larger peak.

The relative widths and amplitudes of the features reflect both the physics of interaction and the detector response. NaI(Tl) detectors exhibit intrinsic energy broadening because the number of scintillation photons produced per absorbed energy is finite and statistical: if N scintillation photons are produced on average, the relative fluctuation scales as $\sigma_N/N \sim 1/\sqrt{N}$; since $N \propto E$, the energy resolution (often quantified as $R = \text{FWHM}/E$) improves slowly with energy and is significantly poorer than semiconductor detectors. In addition to photon statistics, PMT gain variations, electronic noise, the finite SCA channel width and pileup all broaden peaks and reduce peak-to-background ratios. Thus the photopeak, though the most distinct full-energy feature, is broadened and smaller in area than one might expect purely from interaction cross sections.

Finally, the backscatter feature is broader and often larger in integrated counts than the photopeak for several reasons. First, the backscatter feature is not a single monoenergetic feature but a convolution of photons scattered from many different locations and materials with a range of scattering angles close to 180°; small deviations from exact backscatter and subsequent partial energy deposition produce a spread of pulse heights, so the backscatter feature appears as a broad hump rather than a narrow peak. Second, the geometric solid angle and effective cross section for scattering in surrounding structures can be large, so the flux of backscattered photons into the detector can exceed the flux of events that deposit the full 662 keV in a single interaction; consequently the integrated counts in the backscatter feature may be comparable to or larger than those in the photopeak. Third, at the lower energies of backscattered photons the detector photoelectric cross

section increases, raising the probability that an incoming scattered photon will be absorbed and counted (which increases the apparent height of the backscatter feature relative to the high-energy photopeak where Compton scattering in the crystal is more likely than single-step photoelectric absorption). Taken together, these geometric and interaction-probability factors produce the observed broad, sometimes large backscatter feature compared with the narrower photopeak.

In summary, the spectrum exhibits the expected photopeak at 662 keV, the Compton continuum and edge (with the edge near ~ 478 keV deposited energy), the characteristic X-ray peak at ~ 30 keV, and a broad backscatter feature at lower energy with a backscatter peak at ~ 184 keV. The shapes and relative amplitudes of these features are governed by the Compton/photoelectric cross sections, detector statistical resolution, PMT/electronics broadening, and the experimental geometry which controls the production of backscattered photons.

5.3 Fitting the Photopeak region of the spectrum

We will use a combination of Gaussian and Linear fit for the photopeak region. Such a fit would be described by the equation:

$$y(x) = Ae^{-\frac{(x-x_0)^2}{2\sigma^2}} + mx + c \tag{5.3.1}$$

where A, x_0 and σ are respectively the amplitude, centroid and standard deviation of the gaussian and m and c are respectively the slope and y-intercept of the straight line. Using this equation, the fitted graph of the region near photopeak is shown in Figure 7.

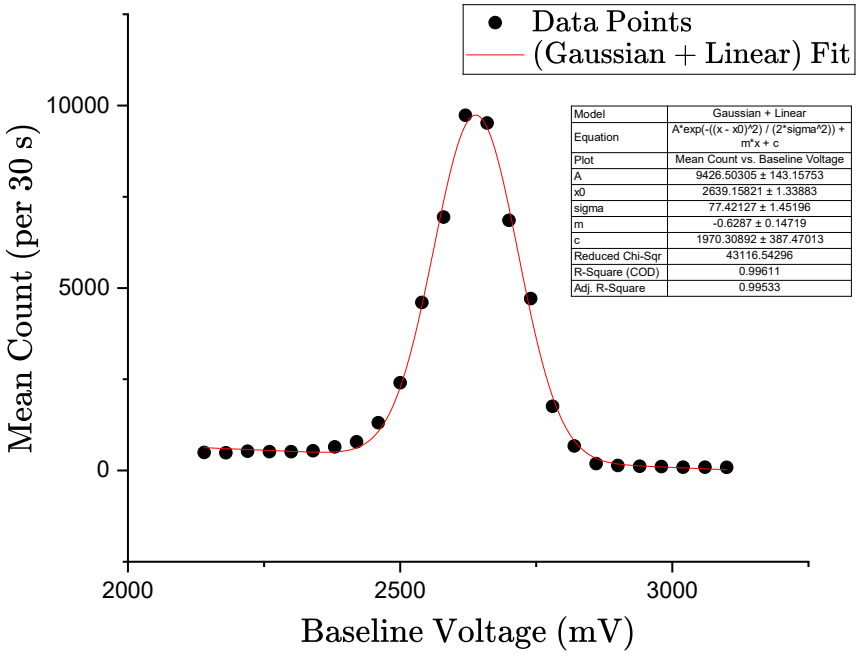

Figure 7: (Gaussian + Linear) Fit of the Photopeak region

5.4 Quantitative analysis of the graph

i) Full Width Half Maximum FWHM

We will first find the Full Width Half Maximum (FWHM) in Figure 7 by substituting $y(x) = 0.5A$ for the Gaussian part in Eq. (5.3.1):

$$\begin{aligned} \Rightarrow \qquad 0.5A &= Ae^{-\frac{(x-x_0)^2}{2\sigma^2}} \\ \Rightarrow \qquad \ln 0.5 &= -\frac{(x-x_0)^2}{2\sigma^2} \\ \Rightarrow \qquad (x-x_0)^2 &= 2\sigma^2 \ln 2 \\ \Rightarrow \qquad x &= x_0 \pm \sigma\sqrt{2\ln 2} \end{aligned} \tag{5.4.1}$$

We have two points on the gaussian curve given by Eq. (5.4.1) which corresponds to the half maximum (for the gaussian part). The FWHM is thus given by the distance between them as follows:

$$\begin{aligned} \text{FWHM} &= 2\sigma\sqrt{2\ln 2} \\ &\approx 2.355\sigma \\ &\approx 182.327 \qquad (\because \sigma \approx 77.421 \text{ from Figure 7}) \end{aligned}$$

ii) Energy Resolution of the detector

Since Baseline Voltage is proportional to the Energy, we have Energy Resolution R of the detector as follows:

$$\begin{aligned} R &= \frac{\Delta E}{E} \times 100\% \\ &= \frac{\Delta V}{V} \times 100\% \\ &= \frac{\text{FWHM}}{x_0} \times 100\% \\ &= \frac{182.327}{2639.158} \times 100\% \qquad (\because x_0 \approx 2639.158 \text{ from Figure 7}) \\ &\approx 6.909\% \end{aligned}$$

iii) Mapping Compton Edge Energy to Baseline Voltage

We know $mc^2 = 0.511$ MeV and $E_\gamma = 0.6617$ MeV. Using this we compute:

$$E_c = \frac{2E_\gamma^2}{2E_\gamma + mc^2} = \frac{2 \times 0.6617^2}{2 \times 0.6617 + 0.511} = 0.477 \text{ MeV}$$

In terms of baseline voltage it should be

$$2639.158 \times \frac{0.477}{0.6617} \approx 1900 \text{ mV}$$

which is consistent with Figure 6.

iv) Mapping Backscatter Peak Energy to Baseline Voltage

$$E_{bc} = \frac{mc^2 E_\gamma}{2E_\gamma + mc^2} = \frac{0.511 \times 0.6617}{2 \times 0.6617 + 0.511} = 0.184 \text{ MeV}$$

In terms of baseline voltage it should be

$$2639.158 \times \frac{0.184}{0.6617} \approx 740 \text{ mV}$$

which is consistent with Figure 6 within experimental error.

6 Sources of Errors

In this experiment, both systematic and random errors influence the measurement of the ^{137}Cs gamma-ray spectrum and the determination of the detector energy resolution. A detailed discussion of possible sources of errors is given below.

6.1 Systematic Errors

- **Energy calibration uncertainty:** The baseline voltage was linearly mapped to gamma-ray energy using the 662 keV photopeak. Any misidentification of the centroid or non-linearity in the electronics introduces a bias in all derived energies. Using only one calibration point increases this uncertainty.
- **Photomultiplier tube (PMT) gain drift:** The PMT gain depends strongly on applied high voltage and ambient temperature. Small drifts during data collection shift peak positions, leading to systematic errors in energy calibration.
- **Detector non-uniformity:** The NaI(Tl) crystal does not have uniform light collection efficiency throughout its volume. Photons generated at different positions in the crystal may produce different output signals even for identical deposited energies.
- **SCA linearity and stability:** The Single Channel Analyzer thresholds may drift with temperature or bias voltage. Non-linearity in threshold response can distort the reconstructed spectrum.
- **Dead-time and pile-up effects:** At high count rates, two or more pulses may overlap (pile-up), or the system may fail to register events during dead-time. Both effects distort peak areas and relative intensities.
- **Background radiation and scattering:** Environmental gamma rays and cosmic rays contribute to the low-energy continuum. Scattering from the laboratory walls, detector housing, and table increases the intensity of the backscatter hump, altering relative peak intensities.
- **Finite energy resolution:** The intrinsic broadening of NaI(Tl) detectors limits the precision of peak position and width determination. This is not an error in the measurement itself but a systematic limitation of the detector technology.
- **Electronic instabilities:** Fluctuations in amplifier gain, baseline shifts, or noise pickup from nearby electrical equipment can cause distortions in peak shape and width.

6.2 Random Errors

- **Statistical fluctuations in scintillation and photoelectron emission:** Even for identical energy deposits, the number of scintillation photons and photoelectrons follows Poisson statistics, producing variation in pulse height.

- **Fit uncertainties:** The Gaussian+Linear fit introduces parameter uncertainties in centroid (x_0), width (σ), and amplitude (A). These propagate into the derived FWHM and resolution.
- **Electronic noise:** Random fluctuations in preamplifier and amplifier stages cause small baseline variations, broadening the observed spectrum.
- **Operator errors:** Human errors in setting discriminator windows, recording counts, or plotting data may contribute to small random deviations.
- **Electronic noise variability:** Short-term fluctuations in amplifier noise contribute to peak broadening and can introduce significant errors in measurement.

7 Result

The main quantitative results obtained from the analysis are summarized below:

- The photopeak centroid was determined at $x_0 \approx 2639.16$ mV.
- The Gaussian width was $\sigma \approx 77.42$ mV, giving a full width at half maximum:

$$\text{FWHM} = 2.355\sigma \approx 182.33 \text{ mV}$$

- The detector energy resolution at 662 keV was:

$$R = \frac{\Delta E}{E} \times 100\% = \frac{\text{FWHM}}{x_0} \times 100\% \approx 6.91\%$$

- The Compton edge was calculated as $E_{\text{CE}} \approx 478$ keV, corresponding to ~ 1900 mV, consistent with observations.
- The backscatter peak energy was $E_{\text{BS}} \approx 184$ keV, corresponding to ~ 740 mV, which matched well with the experimental spectrum within experimental limits.
- A low-energy fluorescence peak around $\sim$ 30–35 keV was also visible, attributed to Ba K X-rays.

8 Conclusion

The experiment successfully demonstrated the measurement of the gamma-ray spectrum of ^{137}Cs using a NaI(Tl) scintillation detector, photomultiplier tube, and Single Channel Analyzer. The major features of the spectrum were clearly identified:

- The full-energy photopeak at 662 keV.
- The Compton continuum and its edge near 478 keV.
- The backscatter peak around 184 keV.
- The characteristic X-ray peak around 30–35 keV.

The detector resolution was measured to be $R \approx 6.9\%$ at 662 keV, which falls within the expected range of 6–10% for NaI(Tl) detectors. This confirms the proper functioning of the detector and validates the experimental analysis.

Future improvements:

- Use of a multichannel analyzer (MCA) would allow simultaneous acquisition of the entire spectrum, eliminating the need for stepwise SCA scanning.
- Longer counting times would improve statistics, reducing uncertainty.
- Additional shielding around the detector would suppress background and reduce the backscatter feature.
- Employing a semiconductor detector such as HPGe would provide superior resolution, allowing finer study of spectral features.
- Calibration with multiple gamma sources (e.g. ^{60}Co, ^{22}Na) would reduce systematic calibration uncertainties.

Overall, the experiment demonstrated the key physical processes (photoelectric effect, Compton scattering, backscattering) and the practical limitations of scintillation spectroscopy, providing a clear understanding of gamma-ray detection and spectral analysis.

References

1. G. F. Knoll, *Radiation Detection and Measurement*, 4th ed., Wiley, 2010.
2. C. Grupen and B. Shwartz, *Particle Detectors*, 2nd ed., Cambridge University Press.
3. Alpen, E. L. *Radiation Biophysics*, 2nd ed., Academic Press, San Diego, CA, 1998.
4. Turner, J. E. *Atoms, Radiation, and Radiation Protection*, 2nd ed., Wiley-Interscience, New York, 1995.
5. Krane, K. S., *Introductory Nuclear Physics*, Wiley, 1987.
6. Firestone, R. B., and V. S. Shirley (eds.), *Table of Isotopes*, 8th edition, Wiley-Interscience, 1996.
7. NuDat 3.0, National Nuclear Data Center (NNDC), Brookhaven National Laboratory.
8. Leo, W. R., *Techniques for Nuclear and Particle Physics Experiments*, Springer, 1994.